Structure of the Human Primosome Elongation Complex

Ci Ji Lim (ciji.lim@wisc.edu)
University of Wisconsin-Madison https://orcid.org/0000-0003-3327-1926
Qixiang He
University of Wisconsin-Madison https://orcid.org/0000-0002-0738-679X
Andrey Baranovskiy
University of Nebraska Medical Center
Lucia Morstadt
University of Nebraska Medical Center
Alisa Lisova
University of Nebraska Medical Center
Nigar Babayeva
University of Nebraska Medical Center
Benjamin Lusk
University of Wisconsin-Madison
Tahir Tahirov
University of Nebraska Medical Center https://orcid.org/0000-0002-1238-0069

Brief Communication

Keywords:

Posted Date: July 13th, 2022

DOI: https://doi.org/10.21203/rs.3.rs-1650573/v1

Version of Record: A version of this preprint was published at Nature Structural & Molecular Biology on April 17th, 2023. See the published version at https://doi.org/10.1038/s41594-023-00971-3.

Abstract

The synthesis of RNA-DNA primer by primosome requires coordination between primase and DNA polymerase α subunits, which is accompanied by unknown architectural rearrangements of multiple domains. Using cryogenic-electron microscope, we solved a 3.6 Å human primosome structure caught at an early stage of RNA primer elongation with deoxynucleotides. The structure confirms a long-standing role of primase large subunit and reveals new insights into how primosome is limited to synthesizing short RNA-DNA primers.

Main

The human primosome, a complex of primase and DNA polymerase α (Polα), provides the RNA-DNA primer to initiate synthesis during DNA replication[1,2]. It is also involved in other DNA transactions, such as telomere maintenance[3-5], DNA damage repair[6], and innate immunity[7-9]. The biomedical importance of the primosome is evident with it being an emerging target for anticancer therapy[10]. The primosome holds a unique functional role in molecular biology due to its ability to *de novo* synthesize a short RNA primer by primase, comprised of catalytic p49 and large p58 subunits, and then switching it to a two-subunit (catalytic p180 and accessory p70) Pola complex for extension with DNA[1,2,11].

Structure-function studies of the primosome have provided much understanding to how the enzyme performs its catalytic actions, but most of these findings are limited to the context of individual domains or subunits, or subcomplexes[12-21]. Clearly, to understand how primosome makes the RNA-DNA primer, it is important to study the enzyme as a heterotetrametric complex. But it is understandably challenging to elucidate structural details of the flexibly tethered primosome complex[22,23]. Indeed, till recently, only the apo state structure of the human primosome has been solved[20,24]. The enzyme apo-state revealed an inhibitory compact structure that possibly explains how the primase domain can act first on a template[1]. A recent cryogenic-electron microscopy (cryo-EM) structure of the human primosome caught in its preinitiation state with its single-stranded DNA-binding accessory protein, CST, provides critical insights into the enzyme's RNA primer synthesis mechanism[25]. Despite these recent advances, the structural details of the primosome in its DNA elongation state remain unclear. In this work, we report the cryo-EM structures of the human primosome trapped in the elongation state, which reveals an architecture different from the enzyme apo[20] or preinitiation[25] states and provides new insights into how the enzyme rearranges to accommodate RNA-DNA primer elongation and facilitate DNA synthesis termination.

We reconstituted the elongation complex by incubating a recombinant human primosome complex with dATP and a DNA template annealed to the 12-mer RNA-DNA primer that has a dideoxycytosine at the 3'-end to prevent further primer extension (**Extended Data Table 1**). Single-particle cryo-EM analysis yielded two major elongation complexes; a $p180_{core}$-$p58_C$ binary complex (Elongation complex I, EC-I; **Fig. 1a**) and an intact four-subunit complex (Elongation complex II, EC-II; **Fig. 1b**), both bound to the template:primer. They were solved at 3.4 and 3.6 Å global resolution for EC-I and EC-II respectively,

allowing us to determine their atomic models (**Fig. 1c**; **Extended Data Figs. 1 and 2 and Supplementary Table 2**).

Both complexes bind the template:primer in similar fashion, with the $p58_C$ domain binding the primer's 5'-triphosphate group while the $p180_{core}$ domain engaging the primer 3' end (**Fig. 1d**). Comparison with the crystal structures of either template:primer-bound $p180_{core}$[21] or template:primer-bound $p58_C$[20] revealed that parts of the duplex are structurally well-conserved around areas interacting with the proteins, while some deviations are observed in remote areas (**Extended Data Fig. 3**). Since EC-I and EC-II shares the same template:primer interactions, it is possible that EC-I is a subcomplex of EC-II that was broken off during cryo-EM sample vitrification.

Our elongation complex structures provide the first direct evidence showing that the $p58_C$ domain remains bound to the template:primer after its handover from p49 to $p180_{core}$, and this engagement persists at least during four cycles of DNA polymerization. This continued primer 5'-end engagement by the $p58_C$ domain is consistent with past studies showing that this domain has high affinity to the template:primer (*Kd* ~ 36 nM)[26], is essential for the internal primer handover[27,28] and is compatible with primer handover model that was generated without accessory proteins[1,20]. But then, why would the $p58_C$ domain persists in holding onto the template:primer after DNA elongation has started? We think this could be a fail-safe mechanism that prevents the catastrophic loss of the template:primer in an event when $p180_{core}$ releases the molecule.

The EC-II complex revealed that the platform domain, p49-$p58_N$-$p180_C$-p70, serves as a scaffold supporting the $p180_{core}$-$p58_C$-template:primer complex (**Fig. 2a-c**). Comparison with the apo state structure[20] revealed a large rearrangement in the overall conformation of the primosome as it progressed to an elongation state (**Extended Data Fig. 4**). Within the platform domain, the disc-like $p180_C$-p70 was rotated 37° relative to its position in the apo state (**Extended Data Fig. 5**). The thumb subdomain of $p180_{core}$ is wedged between the p49 and $p58_N$ domains of primase, fixing the position of $p180_{core}$ relative to the platform (**Fig. 2a**).

Two new interaction sites, identified from the EC-II structure, seemly support this novel elongation complex conformation (**Fig. 2a-c**); in one interaction area, interdomain hydrogen bonds are formed with participation of p49's G97 backbone oxygen, and the sidechains of K95 and Q100 with the side chains of S1127 and E1118 of $p180_{core}$ respectively. In another area, R235 of the $p58_N$ domain forms a salt bridge with E1121 of $p180_{core}$; S113 of $p58_N$ interacts with D1242 and T1244 of $p180_{core}$ (**Fig. 2b**). In addition, the sidechain of L96 from the p49 subunit is inserted into the hydrophobic pocket at surface of $p180_{core}$ (L1087, I1119, V1128 and hydrophobic parts of D1090 and T1091) (**Fig. 2c**).

To explore the role of the newly-identified platform-$p180_{core}$ interactions in primer DNA elongation, we introduced multiple point mutations in two subunits of primase, $p49_{K95E/L96A}$ and $p58_{R235E}$, intended to disrupt $p180_{core}$ docking on the platform (**Fig. 2d**). In our single-turnover trapping assay, the mutations

resulted in longer RNA-DNA primers being made by the enzyme (**Fig. 2d, lane 3 compared to lane 2 and 2e**). For example, the amount of the 41-mer primer is four times higher in the case of the mutated primosome (**Fig. 2e**). In the absence of a DNA trap, we observed a similar increase in the level of a 41-mer product (**Fig. 2d, lane 4 compared to lane 1**), which is ~three-fold higher in the case of the mutant (**Fig. 2e**).

Our structure-guided mutation studies showed that the platform-p180$_{core}$ interaction of EC-II is important for preventing excessive DNA synthesis by Polα. But why would the enzyme evolved to throttle its primer elongation processivity? We believe this early termination behavior works in favor of the replication role of primosome, which is to seed multiple short primers for more processive DNA polymerases to take over. Without proof-reading capability[29], extensive DNA elongation by primosome would lead to additional unnecessary mutations.

Declarations

Acknowledgements

This work was supported by the National Institute of General Medical Sciences grants R35GM127085 to T.H.T. and R00GM131023 to C. L. This research was, in part, supported by the National Cancer Institute's National Cryo-EM Facility at the Frederick National Laboratory for Cancer Research under contract HSSN261200800001E.

Author Information

Contributions

A.G.B developed the protocol for chimeric primer synthesis, carried out the biochemical experiments, and supervised preparation of samples for structural and functional studies. L.M.M, A.E.L, and N.D.B participated in preparation of samples and technical support. Q.H carried out cryo-EM sample preparation, data collection, map construction, structure refinement with supervision by C.L. Q.H and C.L designed the primase mutations. Q.H and B.L.L made the recombinant mutant primase proteins. T.H.T initiated the project, participated in initial model building and refinement, proposing and clarifying the mechanism of termination with the help of team members. T.H.T and C.L. wrote the manuscript with support from A.G.B and Q.H.

Corresponding authors

Correspondence to C.L. (ciji.lim@wisc.edu) or T.H.T. (ttahirov@unmc.edu).

Ethics declarations

The authors declare no competing interests.

Data availability

The cryo-EM maps of the human primosome elongation complexes have been deposited to the Electron Microscopy Data Bank (EMDB) under the accession code EMD-XXX (EC-I) and EMD-YYY (EC-II). The corresponding atomic coordinates are deposited in the RSCB Protein Data Bank under the accession code XXXX (EC-I) and YYYY (EC-II).

References

1. Baranovskiy, A. G. & Tahirov, T. H. Elaborated Action of the Human Primosome. Genes (Basel) **8**, doi:10.3390/genes8020062 (2017).
2. Pellegrini, L. The Pol alpha-primase complex. Subcell Biochem **62**, 157–169, doi:10.1007/978-94-007-4572-8_9 (2012).
3. Lim, C. & Cech, T. R. Shaping human telomeres: from shelterin and CST complexes to telomeric chromatin organization. Nat Rev Mol Cell Biol **22**, 283–298, doi:10.1038/s41580-021-00328-y (2021).
4. Fan, X. & Price, C. M. Coordinate regulation of G- and C strand length during new telomere synthesis. Mol Biol Cell **8**, 2145–2155, doi:10.1091/mbc.8.11.2145 (1997).
5. Reveal, P. M., Henkels, K. M. & Turchi, J. J. Synthesis of the mammalian telomere lagging strand in vitro. J Biol Chem **272**, 11678–11681, doi:10.1074/jbc.272.18.11678 (1997).
6. Mirman, Z. *et al.* 53BP1-RIF1-shieldin counteracts DSB resection through CST- and Polalpha-dependent fill-in. Nature **560**, 112–116, doi:10.1038/s41586-018-0324-7 (2018).
7. Starokadomskyy, P. *et al.* DNA polymerase-alpha regulates the activation of type I interferons through cytosolic RNA:DNA synthesis. Nat Immunol **17**, 495–504, doi:10.1038/ni.3409 (2016).
8. Kilkenny, M. L. *et al.* Structural basis for the interaction of SARS-CoV-2 virulence factor nsp1 with DNA polymerase alpha-primase. Protein Sci, doi:10.1002/pro.4220 (2021).
9. Tang, L., Sheraz, M., McGrane, M., Chang, J. & Guo, J. T. DNA Polymerase alpha is essential for intracellular amplification of hepatitis B virus covalently closed circular DNA. PLoS Pathog **15**, e1007742, doi:10.1371/journal.ppat.1007742 (2019).
10. Han, T. *et al.* The antitumor toxin CD437 is a direct inhibitor of DNA polymerase alpha. Nat Chem Biol **12**, 511–515, doi:10.1038/nchembio.2082 (2016).
11. Doublie, S. & Zahn, K. E. Structural insights into eukaryotic DNA replication. Front Microbiol **5**, 444, doi:10.3389/fmicb.2014.00444 (2014).
12. Sauguet, L., Klinge, S., Perera, R. L., Maman, J. D. & Pellegrini, L. Shared active site architecture between the large subunit of eukaryotic primase and DNA photolyase. PLoS One **5**, e10083, doi:10.1371/journal.pone.0010083 (2010).
13. Vaithiyalingam, S., Warren, E. M., Eichman, B. F. & Chazin, W. J. Insights into eukaryotic DNA priming from the structure and functional interactions of the 4Fe-4S cluster domain of human DNA primase.

Proc Natl Acad Sci U S A **107**, 13684–13689, doi:10.1073/pnas.1002009107 (2010).

14. Agarkar, V. B., Babayeva, N. D., Pavlov, Y. I. & Tahirov, T. H. Crystal structure of the C-terminal domain of human DNA primase large subunit: implications for the mechanism of the primase-polymerase alpha switch. Cell Cycle **10**, 926–931, doi:10.4161/cc.10.6.15010 (2011).
15. Kilkenny, M. L., Longo, M. A., Perera, R. L. & Pellegrini, L. Structures of human primase reveal design of nucleotide elongation site and mode of Pol alpha tethering. Proc Natl Acad Sci U S A **110**, 15961–15966, doi:10.1073/pnas.1311185110 (2013).
16. Perera, R. L. *et al.* Mechanism for priming DNA synthesis by yeast DNA polymerase alpha. Elife **2**, e00482, doi:10.7554/eLife.00482 (2013).
17. Baranovskiy, A. G. *et al.* Structural basis for inhibition of DNA replication by aphidicolin. Nucleic Acids Res **42**, 14013–14021, doi:10.1093/nar/gku1209 (2014).
18. Vaithiyalingam, S. *et al.* Insights into eukaryotic primer synthesis from structures of the p48 subunit of human DNA primase. J Mol Biol **426**, 558–569, doi:10.1016/j.jmb.2013.11.007 (2014).
19. Baranovskiy, A. G. *et al.* Crystal structure of the human primase. J Biol Chem **290**, 5635–5646, doi:10.1074/jbc.M114.624742 (2015).
20. Baranovskiy, A. G. *et al.* Mechanism of Concerted RNA-DNA Primer Synthesis by the Human Primosome. J Biol Chem **291**, 10006–10020, doi:10.1074/jbc.M116.717405 (2016).
21. Baranovskiy, A. G. *et al.* Activity and fidelity of human DNA polymerase alpha depend on primer structure. J Biol Chem **293**, 6824–6843, doi:10.1074/jbc.RA117.001074 (2018).
22. Klinge, S., Nunez-Ramirez, R., Llorca, O. & Pellegrini, L. 3D architecture of DNA Pol alpha reveals the functional core of multi-subunit replicative polymerases. EMBO J **28**, 1978–1987, doi:10.1038/emboj.2009.150 (2009).
23. Nunez-Ramirez, R. *et al.* Flexible tethering of primase and DNA Pol alpha in the eukaryotic primosome. Nucleic Acids Res **39**, 8187–8199, doi:10.1093/nar/gkr534 (2011).
24. Kilkenny, M. L. *et al.* Structural basis for the interaction of SARS-CoV-2 virulence factor nsp1 with DNA polymerase alpha-primase. Protein Sci **31**, 333–344, doi:10.1002/pro.4220 (2022).
25. He, Q., Lin, X., Chavez, B. L., Lusk, B. L. & Lim, C. J. Structure of human CST-pol-α/primase bound to a telomeric overhang poised for initiation of telomere C-strand synthesis. *bioRxiv*, 2021.2012.2016.472968, doi:10.1101/2021.12.16.472968 (2021).
26. Baranovskiy, A. G. *et al.* Insight into the Human DNA Primase Interaction with Template-Primer. J Biol Chem **291**, 4793–4802, doi:10.1074/jbc.M115.704064 (2016).
27. Sheaff, R. J., Kuchta, R. D. & Ilsley, D. Calf thymus DNA polymerase alpha-primase: "communication" and primer-template movement between the two active sites. Biochemistry **33**, 2247–2254, doi:10.1021/bi00174a035 (1994).
28. Arezi, B., Kirk, B. W., Copeland, W. C. & Kuchta, R. D. Interactions of DNA with human DNA primase monitored with photoactivatable cross-linking agents: implications for the role of the p58 subunit. Biochemistry **38**, 12899–12907, doi:10.1021/bi9908991 (1999).

29. Reijns, M. A. M. *et al.* Lagging-strand replication shapes the mutational landscape of the genome. Nature **518**, 502–506, doi:10.1038/nature14183 (2015).
30. Liu, H. & Naismith, J. H. An efficient one-step site-directed deletion, insertion, single and multiple-site plasmid mutagenesis protocol. BMC Biotechnol. **8**, 91 (2008).
31. Baranovskiy, A. G. *et al.* Crystallization and preliminary X-ray diffraction analysis of human DNA primase. Acta Crystallogr F Struct Biol Commun **70**, 206–210, doi:10.1107/S2053230X13034432 (2014).
32. Zhang, Y., Baranovskiy, A. G., Tahirov, T. H. & Pavlov, Y. I. The C-terminal domain of the DNA polymerase catalytic subunit regulates the primase and polymerase activities of the human DNA polymerase alpha-primase complex. J Biol Chem **289**, 22021–22034, doi:10.1074/jbc.M114.570333 (2014).
33. Mizuno, T. *et al.* The intrinsically disordered N-terminal region of mouse DNA polymerase alpha mediates its interaction with POT1a/b at telomeres. Genes Cells **26**, 360–380, doi:10.1111/gtc.12845 (2021).
34. Noble, A. J. *et al.* Reducing effects of particle adsorption to the air-water interface in cryo-EM. Nat Methods **15**, 793–795, doi:10.1038/s41592-018-0139-3 (2018).
35. Punjani, A., Rubinstein, J. L., Fleet, D. J. & Brubaker, M. A. cryoSPARC: algorithms for rapid unsupervised cryo-EM structure determination. Nat Methods **14**, 290–296, doi:10.1038/nmeth.4169 (2017).
36. Punjani, A., Zhang, H. & Fleet, D. J. Non-uniform refinement: adaptive regularization improves single-particle cryo-EM reconstruction. Nat Methods **17**, 1214–1221, doi:10.1038/s41592-020-00990-8 (2020).
37. Pettersen, E. F. *et al.* UCSF ChimeraX: Structure visualization for researchers, educators, and developers. Protein Sci **30**, 70–82, doi:10.1002/pro.3943 (2021).
38. Emsley, P., Lohkamp, B., Scott, W. G. & Cowtan, K. Features and development of Coot. Acta Crystallogr D Biol Crystallogr **66**, 486–501, doi:10.1107/S0907444910007493 (2010).
39. Afonine, P. V. *et al.* Real-space refinement in PHENIX for cryo-EM and crystallography. Acta Crystallogr D Struct Biol **74**, 531–544, doi:10.1107/S2059798318006551 (2018).

Methods

Protein expression and purification

The triple primase mutant $p49_{K95E/L96A}/p58_{R235E}$ was generated in this work by site mutagenesis protocol according to a published protocol[30]. Expression and purification to homogeneity of the human primase heterodimer[31] and human primosome (p49-p58-p180-p70)[32] have been described elsewhere. The N-terminal residues 1-334 of p180 has been deleted because it is poorly folded[33] and is not required for activity[20] and interaction with other primosome accessory proteins[25].

Oligonucleotides for structural and functional studies

Sequences of all oligonucleotides are provided in Extended Data Table 1. Oligonucleotides without 5'-triphosphate were obtained from IDT Inc. The 5-mer RNA primer P5 containing the 5'-triphosphate (5'-pppGGCGG) was obtained as described previously using DNA duplex T3:P4 and RNA polymerase of bacteriophage T7[26]. Template:primers containing P2 or P3 were obtained by ligation using the corresponding template, P5, RNA ligase 2 of bacteriophage T4 (New England BioLabs Inc.), and P6 or P7, respectively. Reactions were incubated for one hour at 25 ºC and ligated duplexes were purified by 1 mL monoQ column (Cytiva) at 50 ºC.

Sample preparation for cryo-EM studies

The primosome elongation complex was obtained by mixing recombinant human primosome with T2:P3 duplex at a molar ratio of 1:1 in a buffer containing 20 mM Tris-HCl, pH 7.7, 100 mM KCl, 1% (v/v) glycerol, 1 mM TCEP, 1.5 mM $CaCl_2$ and 1.7 mM dATP. The reconstituted elongation complex was concentrated to 8 mg/mL and flash-frozen using as 5 µl aliquots before storage in a -80 °C freezer. The frozen samples were thawed just before cryo-EM grids preparation. To prevent sample damage during cryo-EM grid vitrification, a final 8 mM CHAPSO[34] was added to the elongation complex sample before applying 3.5 mL of the sample to a glow-discharged holey EM grid (Quantifoil QF 1.2/1.3, 300 mesh). The grid was blotted for 3.5 s at 4 °C and 95 % relative humidity and plunge-frozen with liquid ethane as cryogen using the Vitrobot machine (FEI, ThermoFisher Inc., USA).

Cryo-EM data collection and processing

A total of 13,243 movies were collected on a Titan Krios transmission electron microscope (FEI, ThermoFisher Inc., USA) at the National Cryo-Electron Microscope Facility at the National Cancer Institute of the National Institute of Health (NIH). The movies were imaged at a nominal pixel resolution of 1.12 Å/pixel using a K3 direct electron detector in counting mode and energy filter at 20 eV (Gatan, USA). Each movie is collected across 40 frames with a total electron dose of 50 e-/$Å^2$. The movies were aligned and their CTF parameters calculated using CryoSparc2[35] patch motion-correction and CTF estimation. 12,168 micrographs remained after curation and from these micrographs, 2,522,283 particles were picked and extracted at 4X binning (4.48 Å/pixel). The particles were subjected to a single round of 2D classification to remove most junk particles/ice contaminations. Selected particles (899,717 particles) were further sorted into four separate reference-free 3D classes using CryoSparc2 *ab initio* modeling. Two distinct conformations of the elongation complexes (EC-I and EC-II) were resolved in this step.

The particles from these two classes (total of 589,593 particles) were re-extracted at the original pixel size before undergoing another round of 4-classes *ab initio* modeling. This step yielded the final particles subsets for EC-I and EC-II. 32.3 % of the particles (151,102 particles) belong to EC-I while 41.9 % of the particles (199,286 particles) belong to EC-II. Non-uniform refinement with per-particle CTF refinement[36] resulted in a global resolution (reported at FSC = 0.143) of 3.4 Å for EC-I and 3.6 Å for EC-II.

Model building, refinement and validation.

The EC-I and EC-II models were built by docking solved structures of individual domains[20,21] into the cryo-EM maps. Docking was done using ChimeraX software[37]. The elongation complex models were inspected visually with respect to their fit in their respective cryo-EM maps and manually corrected using Coot[38]. The models were then subjected to real-space refinement using the Phenix software[39]. Cryo-EM map to model validation statistics were derived from Phenix's comprehensive validation package.

Primer extension assay

Activity was tested in 10 µl reaction containing 0.6 µM template:primer, 0.2 µM enzyme, 10 µM dNTPs, 0.1 µM [α-^{32}P]-dCTP (3000 Ci/mmol; PerkinElmer, Inc.), 10 µM trap, and the buffer: 30 mM Tris-Hepes, pH 7.8, 120 mM KCl, 30 mM NaCl, 1% glycerol, 2 mM TCEP, 5 mM $MgCl_2$, and 0.2 mg/ml BSA. The trap was a T4:P8 duplex containing the dideoxy-cytosine at the primer 3'-end to make a dead-end complex with Polα. The enzyme was pre-incubated with a template:primer in 5 µl for 1 min on ice and for 10 sec at 35 ºC, then reaction was initiated by addition of 5 µl solution containing dNTPs and trap. Reactions were incubated in PCR tubes on a water bath for 30 sec at 35 °C and stopped by mixing with equal volume of formamide loading buffer (90% v/v formamide, 50 mM EDTA, pH 8, 0.02% Bromophenol blue), heated at 95°C for 1 min, and resolved by 20% Urea-PAGE (UreaGel System (19:1 Acrylamide/Bisacrylamide), National Diagnostics) for 2.5 h at 3000 V. The reaction products were visualized by a phosphorimager (Typhoon FLA 9500, Cytiva). All activity gels were repeated at least two times for reproducibility.

Figures

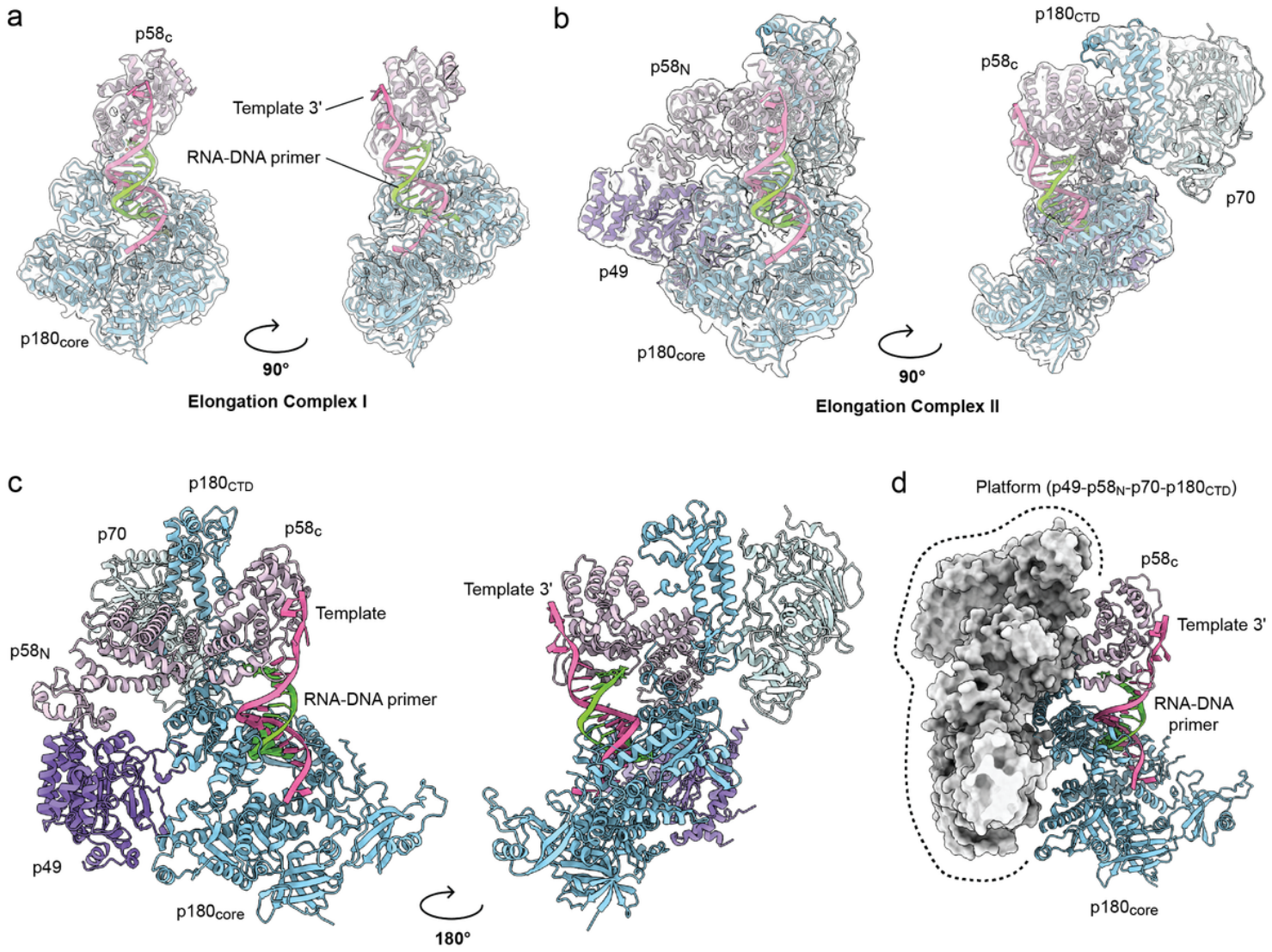

Figure 1

Architecture of human primosome elongation complex. (a) Elongation complex I (EC-I) that consists of polymerase a catalytic domain ($p180_{core}$) co-binding to the template:primer substrate with primase large subunit C-terminal domain ($p58_C$). The model is built based on the cryo-EM map which is semi-transparent in grey. Template (5' - ATAATGGTCGTGCCGCCAATAA - 3') is colored as hot pink while the RNA-DNA primer (5' - ppp*GGCGGCACG*AC/ddC/ - 3') is colored as lawn green. Underlined sequence indicates primer complementary region on the template. RNA portion of the primer is italicized. ddC – dideoxycytidine. **(b)** Elongation complex II (EC-II) consists of all four primosome subunits: p49, p58, p70, and p180. The $p180_{core}$ and $p58_C$ domains bind the template:primer substrate in the same way as EC-I (see panel a). **(c)** Atomic model of EC-II, with all four subunits and the template:primer substrate labeled. Only the $p180_{core}$ and $p58_C$ domains are in contact with the nucleic acid substrate while the rest of the domains/subunits (collectively termed the platform domain) supports the overall structure. **(d)** The platform domain (p49-$p58_N$-p70-$p180_{CTD}$) is depicted as surface representation and colored grey to illustrate its role as a $p180_{core}$-template:primer-$p58_C$ scaffold.

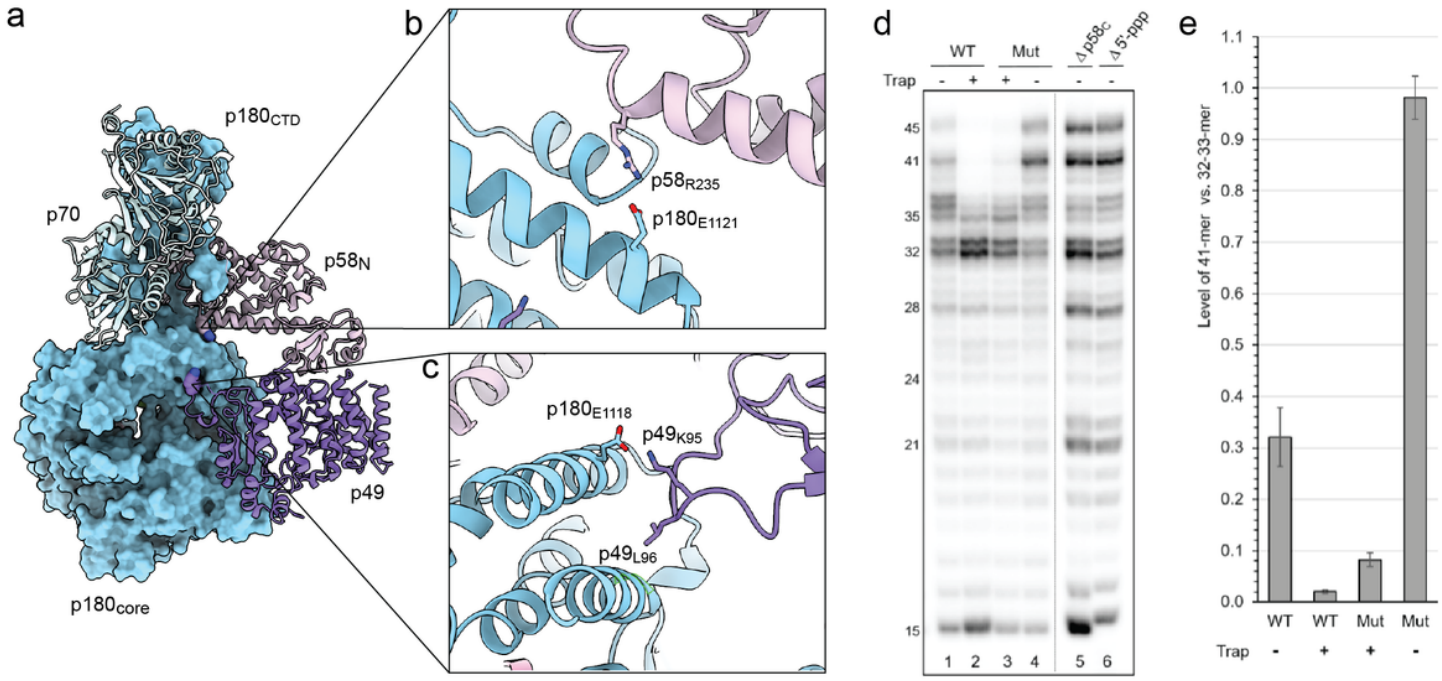

Figure 2

Platform domain interaction with $p180_{core}$ is important for timely termination of RNA-DNA primer synthesis. (a) Intermolecular interactions enabling docking of $p180_{core}$ to the platform. Overall view is shown on the left. Platform is drawn as ribbon cartoons and $p180_{core}$ is drawn as surface. The side chains of residues selected for mutations are shown in spheres. **(b & c)** Close up views of intersubunit interactions in two areas are shown on the right. **(d)** Mutations disrupting the platform-$p180_{core}$ interaction increase processivity of DNA synthesis. Mut - Polα/$p49_{K95E/L96A}$/$p58_{R235E}$. Lane 5 – primosome with deleted $p58_C$. Lane 6 – primer without 5'-triphosphate (T1:P1). T1:P2 was used in reactions corresponding to lanes 1-5. **(e)** Effect of the triple mutation on the level of 41-mer (see the panel d). The data are presented as bar graphs showing the mean ±SD calculated from three independent experiments.

Supplementary Files

This is a list of supplementary files associated with this preprint. Click to download.

- ExtendedData.docx
- ECII.txt